Industrial Crops & Products 188 (2022) 115692

Contents lists available at ScienceDirect

Industrial Crops & Products

journal homepage: www.elsevier.com/locate/indcrop

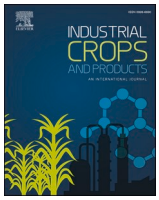

From lignocellulosic biomass to chemical precursors: Simultaneous valorization of furfural and levulinic acid over mesoporous acid catalysts

Jennifer Cueto, Laura Faba, Eva Díaz, Salvador Ordóñez [*,1]

Catalysis, Reactors and Control Research Group (CRC), Dept. of Chemical and Environmental Engineering. University of Oviedo, Julián Clavería s/n, Oviedo 33006, Spain

ARTICLE INFO

Keywords:
Heterogeneous catalysis
Alumina
Green chemistry
Kinetics
Renewable resources

ABSTRACT

This paper analyses the furfural and levulinic acid aldol condensation over mesoporous acid materials. This process is a promising route to obtain chemical feedstock and biofuel precursors from two of the most available bio-platform molecules produced from nonedible lignocellulosic biomass. Different acid solids were tested (ion-exchange resins, MCM, γ-Al_2O_3), obtaining the best results with alumina (γ-Al_2O_3). This material reaches a feasible equilibrium between sustainability (heterogeneous, available, and cheap catalysis, soft temperatures), activity (45 % of levulinic acid conversion, C10s yield of 44 %) and stability (no deactivation observed after four cycles). These results significantly improve those reported in the literature using microporous materials since the adsorption is significantly limited, as demonstrated by the good carbon balance (>95 %), the kinetic model and spent catalyst characterization.

1. Introduction

Levulinic acid (LA) and furfural (FFL) are two of the top ten renewable chemicals produced from lignocellulosic biomass (Werpy and Peterson, 2004). They are the main compounds obtained during (hemi) cellulosic biomass hydrolysis (a typical first stage in a biorefinery scheme). Levulinic acid is produced by the acid-catalyzed dehydration and decomposition of cellulose and hexoses (Zhi et al., 2015; Garcés et al., 2019; Di Bucchianico et al., 2022), whereas furfural is a typical reaction product of hemicelluloses hydrolysis (Cai et al., 2014; Zhang et al., 2017; Wang et al., 2021). Both compounds have five carbon atoms and a high oxygen content, both properties hindering their direct use as fuels or fuel additives. Thus, subsequent steps to increase the carbon length and/or remove oxygen atoms are required.

Aldol condensation is the optimum alternative to generate new carbon-carbon bonds, being a reaction carried out under mild conditions that can be adapted to a wide range of potential reactants (Chheda et al., 2007). This approach has been successfully tested with different biomass-derived platform molecules, as furfurals (Faba et al., 2012; Deng and Amarasekara, 2021), 5-hydroxymethylfurfural (HMF) (Cueto et al., 2017; Malkar et al., 2019) and, to a lower extent, levulinic acid and its dehydrated derived compound, angelica lactone (Amarasekara et al., 2015; Xu et al., 2017; Zhao et al., 2021). A plethora of C7-C15 compounds are obtained by the self- or cross-condensation of these molecules, (the last and most studied alternative implies using a linking molecule -α-H donor- such as acetone, cyclopentanone, etc.) (Li et al., 2018, Deng and Amarasekara, 2021, He et al., 2021). Most of these studies propose the basic mechanism, both homogeneous and heterogeneous catalysts. However, the acid route has been also proposed, as reviewed by *Li and co-workers* (He et al., 2021), concluding that both mechanisms are feasible but, in general terms, the basic one allows working in softer conditions with higher conversions and yields.

In 2016, our research group published a study about the levulinic acid self-condensation using basic mixed oxides (MgAl, MgZr), obtaining C10 compounds and a relevant cyclization, yielding angelica lactone (Faba et al., 2016). The dimerization capacity of this intermediate using K_2CO_3 was previously observed by *Mascal and coworkers,* demonstrating the prevalence of the carboxylic acid activity over the carbonylic one when working with basic materials (Mascal et al., 2014). The acidic route was also studied, obtaining limited yields despite the more severe conditions (130 °C), and the high catalytic loading (Amarasekara et al., 2019). Based on these studies, the potential of the levulinic acid self-condensation is not enough to be competitive, suggesting its cross condensation with furfural as a good alternative (He et al., 2021).

* Corresponding author.
E-mail address: sordonez@uniovi.es (S. Ordóñez).
[1] ORCID: 0000-0002-6529-7066

https://doi.org/10.1016/j.indcrop.2022.115692
Received 22 July 2022; Received in revised form 14 September 2022; Accepted 18 September 2022
Available online 22 September 2022

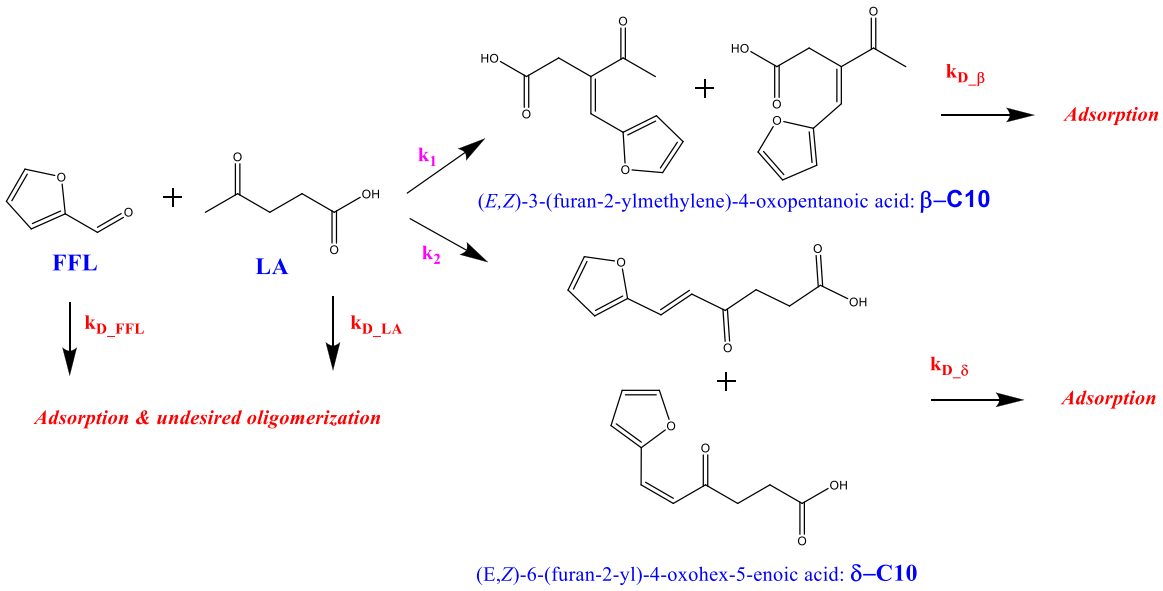

Scheme 1. Proposed reaction network for FFL-LA aldol condensation (Liang et al., 2016).

Considering the potential availability of furfural and levulinic acid, the development of an effective route for their cross-condensation could represent a sustainable process to obtain intermediates in the optimum carbon range (10−15) using non-edible biomass, with a significant reduction in the purification requirements of the hydrolyzed biomass since they can be simultaneously produced (Li et al., 2019). However, the high activity of the carboxylic functionalization of the levulinic acid requires special attention (Xue et al., 2018), restricting the reaction conditions. Aldol condensation between levulinic acid and furfural gives to two furfurylidenelevulinic acid isomers (β-C10 and δ-C10) (Liang et al., 2016), as observed in Scheme 1. These molecules are promising building blocks for obtaining biofuels, polymers and fine chemicals, with a huge range of applications.

The corresponding route using HMF instead of furfural is scarcely studied since the stability of HMF in presence of an acidic medium is very limited, being degraded into levulinic acid. Thus, there is only one study proposing NaOH as the catalyst (Amarasekara et al., 2015), with all the environmental concerns about using homogeneous catalysis.

As to levulinic acid and furfural condensation, base-catalyzed rection pathways, studied with MgO, MgAl, MgZr, ZrO_2, and TiO_2, among others (Liang et al., 2016; Cueto et al., 2020), demonstrates the need of a previous levulinic acid neutralization step (with an inorganic salt) as well as the prevalence of the δ-C10 isomer over the β-C10 (maximum yield of 70.6 % after 3 h at 85ºC with MgO, $\delta/\beta = 4.6$). The subsequent condensation with a second furfural molecule is not reported using solid catalysts, whereas these compounds are selectively produced using NaOH (97.5 % yield of C15 at 50 °C) (Li et al., 2016; Tan et al., 2018). However, the use of NaOH implies relevant technical challenges regarding to corrosiveness, recyclability, and neutralization requirements. Recently, Zhang and coworkers proposed the use of modified chitosan as a basic catalyst; obtaining outstanding yields at room temperature (16 % and 78 % of C10 and C15, respectively) (Zhao et al., 2021).

Furfural and levulinic acid syntheses occur in an acidic medium. Thus, their cross condensation with an acidic catalyst appears to be compatible with the upstream synthesis, minimizing neutralization and purification operations (reducing the energy and material consumption). Moreover, it is expected that the acidic catalyst reduces the interactions with the carboxylic group and the presence of lateral reactions. Thus, acid-promoted condensation was tested over ZnO, Nb_2O_5, and, mainly, different zeolites (H-Y, H-β, H-ZSM-5, H-MOR) (Liang et al., 2016; Cueto et al., 2020), obtaining a more selective process, but with higher activation energies than with the basic approach (temperatures over 120ºC being required to reach similar conversions). The different reaction mechanism in acidic conditions (based on an enol intermediate) promotes the branched isomer (β-C10) over the linear one. Thus, at short times the linear product is not detected (Liang et al., 2016), whereas longer times and more severe conditions stabilize the β/δ ratio in values close to 5 (Cueto et al., 2020).

An intermediate approach with a potassium-modified hierarchical MFI zeolite achieved 70 % of C10, with a total furfural conversion after 9 h at 100ºC, with an intermediate β/δ ratio, in good agreement with the co-presence of basic and acidic sites (Su et al., 2019). In all these cases, the strong acidity of these zeolites, as well as their small pore size, promote lateral reactions and adsorption of reaction intermediates (discrepancies between conversion and C10 yield) that question the technical viability of a future scale-up in terms of stability (Cueto et al., 2020). On the other hand, the microporous character of this materials can lead to lower efficiency because of the poor accessibility to active site and the presence of mass-transfer limitations.

Since many of these problems can be solved using mesoporous materials, this work proposes a screening of different cheap, available, commercial, and environmentally friendly mesoporous acid catalysts. The activity is evaluated in terms of morphology and acid site concentration and distribution, comparing the behavior of Al_2O_3, Al-MCM-41, and two acidic resins (Amb-36, Amb IR-120). These materials represent three of the most studied families of acidic catalysts in aldol condensations (Gelbard, 2005; Kikhtyanin et al., 2014; Ramírez et al., 2017; Wen et al., 2020; Pasricha et al., 2022). They cover a huge variety of acidity: strong acidity marked by the presence of -SO_3H functional groups in the case of the resins (Russo et al., 2020), Lewis acid sites in Al_2O_3 (Wang et al., 2013), and a combination of Lewis and Brønsted sites in the case of Al-MCM-41 (Perego and Millini, 2013). The activity of these materials is deeply analyzed, as a function of different reaction conditions (temperature, reaction time, initial reaction rates), studying their activity, selectivity and stability in terms of the combined severity factor, to identify the optimum material considering also the sustainability of the process. All the experimental results were fitted to a kinetic model, establishing the kinetic rate constants required for understanding the involved reactions and scaling up these developments.

2. Material and methods

2.1. Catalysts characterization

Commercial mesoporous materials, γ-Al_2O_3 (BASF, D10–10), Al-MCM-41 (Sigma Aldrich), Amb. IR-120 (Merck) and, Amb. 36 (Sigma Aldrich) have been used in this study. Al_2O_3 and Al-MCM-41 (henceforth MCM) materials have been treated at 550 °C for 5 h in a furnace to clean the surface and remove impurities. Resins have been submerged in a bath containing a solution of 0.1 M HCl to reassure their activation.

Morphological properties (surface area, pore diameter and pore volume) were determined by nitrogen physisorption at − 196 °C using an ASAP 2020 (Micromeritics) static volumetric apparatus after the corresponding degasification step at 110 °C during 6 h. NH_3-temperature programmed desorption (NH_3-TPD) was used to evaluate their acid properties using a Micromeritics TPD/TPR 2900. Pfeiffer Vacuum Omnistar Quadrupole Mass Spectrometer was employed to measure NH3 signal evolution. Materials were heated to 300ºC in helium flow (1 h, 20 mL·min^{-1}) and saturated in NH_3 flow (2.5 % NH_3/He, 20 mL·min-1) at ambient temperature for 15 min. The desorption of the NH_3 with the temperature was then analyzed (from room temperature to 800 °C with a ramp of 5 °C·min^{-1}). The acidity was also measured by titration with NaOH. 25 mg of each catalyst were introduced into 50 mL of 0.1 M solution of NaCl, acidifying the mixture previously with 0.5 mL of 0.1 M HCl. After 3 h of stirring at room temperature, different volumes of 0.1 M NaOH until neutral pH were obtained.

The presence of organic compounds adsorbed on the catalytic surface was corroborated by temperature-programmed oxidation analyses (TPO), using the same instrument as for TPD, measuring the CO_2 signal with the mass spectrometer whereas the spent catalysts were treated in oxygen flow (2 % O_2 in He), increasing the temperature up to 1000 °C at a 2.5 °C·min^{-1} rate.

2.2. Aldol condensation reactions

Furfural (FFL) and levulinic acid (LA) aldol condensation was performed in a 0.5 L stirred batch autoclave reactor equipped with a PID temperature controller and a backpressure regulator (Autoclave Engineers EZE Seal). Firstly, 100 mL of LA (2 M, Sigma Aldrich, 99 %) was neutralized with a 0.1 mol of Na_2CO_3 (Panreac, 99 %) obtaining sodium levulinate, NaLe. The reactor was loaded with 0.25 L of an aqueous solution of FFL (Sigma Aldrich, 99 %) and NaLe solution (5 % wt. of reactants), introducing 1.8 g of catalyst (average diameter of 50–80 μm). The ratio between the reactants is defined for each experiment. The reactor was purged with N_2 and the condensation was carried out under 15 bar of N_2 with a stirring of 1000 rpm, with a temperature range from 125 to 175 °C.

For the reusability studies, the spent catalyst was isolated by filtration, being washed with ethyl acetate and dried overnight at 100ºC and heat treated in a muffle for 3 h at 650 °C.

The evolution of the reaction was followed by taking the liquid samples from a sample port equipped with a filter to prevent the extraction of catalysts and possible solids formed during the reaction. The samples were extracted in ethyl acetate (volume ratio of 1:1) and acidified with HCl (2:1 vol ratio aqueous phase: solution 1 M of HCl). The organic phase was analyzed by GC in a Shimadzu GC-2010 equipped with an FID detector, using a 30 m long CP-Sil 8 CB capillary column. Peak assignment was carried out by GC-MS in a Shimazdu GC/MS QP 2010 Plus Instrument, equipped with a 30 m long TRB-5MS capillary column, using commercial samples for calibration (LA and FFL) or the relative carbon concept for the products (considering FFL as basic compound). The activity results were defined in terms of conversion, atomic yields, carbon balance, and combined severity factor, calculated as follows (Eqs. 1–4):

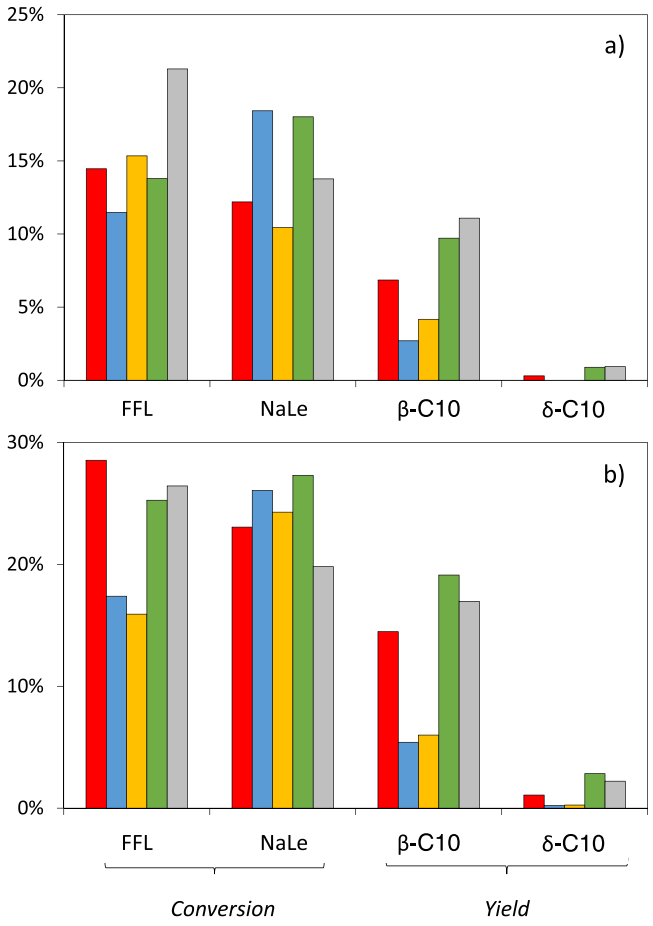

Fig. 1. Main results obtained after (a) 4 h, and (b) 8 h of FFL-NaLe aldol condensation (1:1) at 125ºC using different catalysts (7.2 g/L). Data correspond to ZSM-5 (red), Amb IR-120 (blue), Amb-36 (yellow), MCM (green), and Al_2O_3 (grey).

$$Conversion \quad (\%) = 100 \cdot \frac{(reactant_{t=0} - reactant_t)}{reactant_{t=0}} \tag{1}$$

$$\Psi_{C10} = 100 \cdot \frac{10 \cdot (mol\_\delta C10 + mol\_\beta C10)_t}{(5 \cdot mol\_LA + 5 \cdot mol\_FFL)_{t=0}} \tag{2}$$

$$C.B. = 100 \cdot \frac{10 \cdot (mol\_\delta C10 + mol\_\beta C10)_t + 5 \cdot (mol\_LA + mol\_FFL)_t}{(5 \cdot mol\_LA + 5 \cdot mol\_FFL)_{t=0}} \tag{3}$$

$$CSF = log\left(t \cdot exp^{\left(\frac{T - T_{ref}}{14.75}\right)}\right) \tag{4}$$

Where t is the reaction time (min), T is the temperature (°C), T_ref is the reference temperature (100 °C).

Experimental results were fitted to a kinetic model based on differential equations solved using MATLAB code based on the "lsqcurvefit" function, using the Levengerg-Marquardt algorithm. The fitting of the unknown parameters of the model was accomplished by the least-square method.

3. Results and discussion

3.1. Catalyst screening

The catalytic screening was designed considering several mesoporous materials with different acidity, both in type and strength

Table 1
Summary of main surface chemical properties of the materials used in this work.

Catalyst	ZSM-5	Amb. IR-120	Amb-36	Al_2O_3	MCM
Morphology					
S_{BET} ($m^2 \cdot g^{-1}$)	353	< 1	33	216	1288
$S_{DUBININ}$ ($m^2 \cdot g^{-1}$)	478				
d_p (nm)	8	–	240	88	43
V_{micro} ($cm^3 \cdot g^{-1}$)	0.12	–	–	–	–
V_{meso} ($cm^3 \cdot g^{-1}$)	0.07	–	0.14	0.47	1.67
Acidity (μmol $NH_3 \cdot g^{-1}$)	**350**	–	–	**266**	**434**
Weak (<250ºC)	229			148	257
Medium	121			118	177
Strong (>500ºC)	–			–	–
Acidity (μmol $H^+ \cdot g^{-1}$)		5.3	3.5		
Lewis/Brønsted acidity	1.1[a]	1	1	*All Lewis*[b]	1.04[c]

[a] (Rapado et al., 2021),
[b] (Estevez et al., 2015),
[c] (Schekler-Nahama et al., 1998).

distribution terms: two acidic resins, a mesoporous aluminosilicate (MCM), and γ-Al_2O_3. Considering the low thermal stability of the acidic resins, the reactions were carried out at 125 °C. The experimental results are compared in Fig. 1, including also those obtained with ZSM-5, the optimum microporous material determined in our previous work (Cueto et al., 2020), for comparison purposes. The correct analysis of these results requires the characterization of the surface chemical properties of these materials. The main results are summarized in Table 1.

Significant differences between the materials tested are observed. In the case of both resins (blue and yellow bars), the strong acidity of their sulphonyl functional groups enhances adsorption over the reaction, observing a clear discrepancy between the disappearance of both reactants and the presence of any condensated adduct. Thus, yields of 3 % and 4.2 % of β-C10 are obtained after 4 h, with Amb IR-120 and Amb-36, respectively, without observing the linear adduct. At this time, most of 10 % of furfural has disappeared (in both cases), a percentage that increases up to 18.4 % for the levulinic acid when using the Amb IR-120. In good agreement with these results, the carbon balance closures are quite poor: 87.8 % and 91.3 %, for Amb IR-120 and Amb-36, respectively. Amb IR-120 is more acidic than Amb-36 (5.3 and 3.5 meq $H^+ \cdot g^{-1}$, according to titration with NaOH results), justifying the highest adsorption observed.

After 4 h of reaction, the levulinate adsorption observed with Amb IR-120 is almost double that of the FFL one, whereas the FFL adsorption prevails in the case of Amb-36. However, after 8 h, no differences between these two materials are observed, experimental results being in good agreement with the acidity order. The evolution of the C10 atomic yields is almost negligible, obtaining final values of 5.5 % and 6.2 %, with an almost total absence of δ-C10. These results are in good agreement with the previous literature about the use of other strong-acid cation exchange resins (Liang et al., 2016), suggesting that Brønsted acidity is completely inactive for this condensation.

After 4 h, the mesostructured MCM (green bars) shows a FFL conversion of 13.8 %, observing 10.6 % of total C10s and a clear prevalence of the branched isomer (β/δ ratio of 10.8). This material exhibits the best carbon balance closure (94.7 %), the NaLe adsorption or its lateral reactions being identified as the main undesired effects (18 % of disappearance in 4 h). The surface properties of this material (summarized in Table 1) suggest that the presence of protons on the surface (Brønsted acidity) could partially protonate the levulinate, yielding the initial LA in the reaction medium. At this point, two phenomena are possible: its adsorption on these acidic sites or its cyclization and oligomerization by the Aldol-Michael mechanism (Nieminen et al., 2004; Amarasekara et al., 2019).

The second option is discarded considering the results after 8 h. The discrepancy between theoretical LA conversion and the C10 production

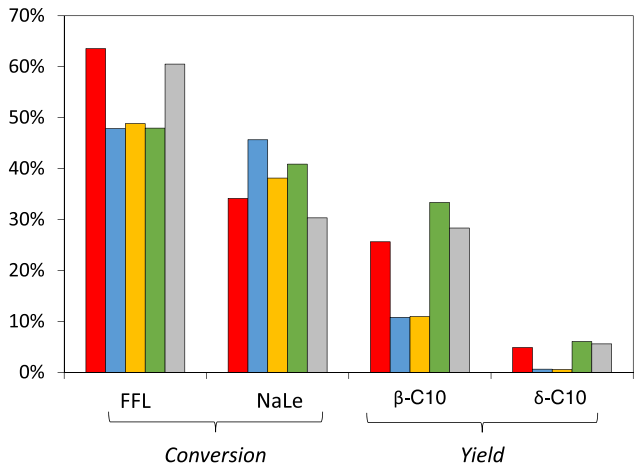

Fig. 2. Main results obtained after 24 h of FFL-NaLe aldol condensation (1:1) at 125ºC using different catalysts (7.2 g/L). Data correspond to ZSM-5 (red), Amb IR-120 (blue), Amb-36 (yellow), MCM (green), and Al_2O_3 (grey).

represents 41 % after 4 h whereas, during the following 4 h, this value decreases to < 1 %. Thus, stable adsorption of LA obtained by the interaction between NaLe and the Brønsted acids of the MCM is proposed, producing the blockage of Brønsted acid sites, Lewis ones being the only active for the aldol condensation. The good strength distribution of acidity justifies the good results obtained with MCM, with a final carbon balance of 95.7 %, obtaining 22 % of C10 after 8 h (β/δ ratio of 6.8).

After 4 h, Al_2O_3 (grey bars) shows the highest furfural conversion (21.3 %), with an almost total correspondence between the total atomic yield to C10 adducts (12 %, β/δ ratio of 12.3) and the levulinic acid conversion (13.4 %). These results are congruent with the good carbon balance closure (94.6 %) obtained with this material, suggesting a low influence of side reactions, the furfural adsorption being the only relevant one under these conditions. These results are justified by the mesoporous character of Al_2O_3 and the subsequent high active sites accessibility, the prevalence of Lewis acidity, as well as the high concentration of weak acid sites, keeping the control of the reaction at the formation of the C10 adducts. In fact, results obtained after 8 h indicate almost 20 % of C10s, with a total correspondence with the NaLe conversion and 96.2 % of carbon balance closure. These results are quite similar to those obtained with MCM, despite the fact that the acidity of Al_2O_3 is almost half of that of the MCM. Moreover, the C10 selectivity is significantly higher than the one reached with ZMS-5, the catalyst with the highest acidity, suggesting that the accessibility to the active sites prevails over the total acidity.

Considering the continuous increasing trend observed for both C10 compounds, longer times were tested, the experimental results being analyzed in Fig. 2.

After 24 h, MCM shows FFL and NaLe conversions of 48 % and 41 %, respectively, with a quite good correspondence with the total C10 production (39.3 % of total yield, β/δ ratio of 5.6) and, subsequently, the carbon balance closure (95 %). Thus, increasing the reaction time is considered a good option to enhance the C10 production, without observing relevant adsorption or lateral reactions. These results are better than those previously reported in the literature using microporous materials (Liang et al., 2016; Cueto et al., 2020). In the case of Al_2O_3, the effect of the reaction time is not so positive, reaching a total yield of 34 % (β/δ ratio of 5). These values do not correspond with the 60.5 % of furfural conversion. This discrepancy, with its effect on the carbon balance (89 %) suggests slow but relevant furfural adsorption (the possible presence of furfural oligomerization is discussed below, see stability section) that discourages this approach to enhance the C10 yield with Al_2O_3 since the catalyst stability could be reduced. No

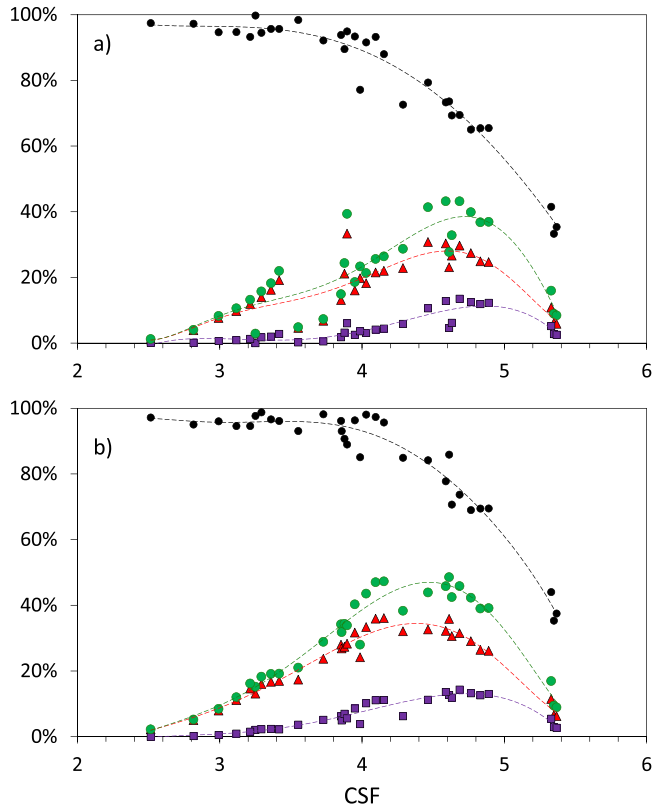

Fig. 3. Analysis of the simultaneous influence of reaction temperature and time in the carbon balance (•), and product yields: β-C10 (▲), δ-C10 (■), and total C10 (●). Results correspond to (a) MCM; (b) Al_2O_3.

improvements were observed in the case of resins. Based on the initial results of the catalytic screening, MCM and Al_2O_3 are selected as catalysts for a deeper study of the influence of reaction conditions. These analyses were done at 8 h considering that the improvements observed in increasing the reaction time to 24 h are not enough to justify this long reaction time.

3.2. Effect of the temperature

Working at higher temperatures allows to improve the activity results, reducing the reaction times required to increase the C10 yield, with a possible positive effect of reducing adsorption effects. Thus, the activity of MCM and Al_2O_3 was tested at 150ºC and 175ºC. Since two parameters are expected to influence on the activity results (reaction time and temperature), their effect must be simultaneously considered. Thus, experimental results are evaluated according to the combined severity factor (CSF), which represents the reaction severity as a function of the reaction temperature and time. This coefficient is adapted from the literature, where a more complex expression simultaneously analyses the effect of different reaction conditions, including temperature, time, and the pH (Choudhury and Mukherjee, 2020). In this work, this expression has been simplified since all the experiments were carried out at the same initial pH. Experimental results are plotted in Fig. 3.

In both cases, high CSF values (>4.3) lead to a decrease in the carbon balance, requiring soft conditions to guarantee a value higher than 85 %. As to the products, the yields of C10 adducts increase with the CSF, reaching a maximum at intermediate CSF values (3.8–4.8 range), with a significant decreasing trend after it. The correspondence between the depletion of the carbon balance and the C10 yields proposes the stable adsorption of these compounds as the main cause. The fast decrease suggests disordered adsorption with oligomerization (discussed in the stability section), discouraging working under these conditions and defining a maximum C10 yield slightly lower than 50 %.

Despite the similar trends observed, some differences between both materials can be highlighted. In the case of MCM, there is not a clear trend of the total C10 (green circles) with the CSF value. This indicates that there is not a good correspondence between values obtained with the same severity if this coefficient is due to the temperature or the time. In fact, for the same CSF value, better yields are obtained when working for long times (>6 h) but at low temperatures. This fact supports the hypothesis of the prevalence of carbon unbalances due to oligomerization, reactions that are promoted by the temperature, with a partial consumption of the C10 produced.

On the other hand, the CSF and yields correspondence is very clear in the case of Al_2O_3. In both cases, the maximum of δ C10 is slightly displaced to higher values for to the β-C10, but its contribution with Al_2O_3 is more significant, reaching a maximum of total C10 of 47 %. This value

Table 2
Kinetic and adsorption rates for the FFL-NaLe aldol condensation with 7.2 g/L of catalyst. Values of ZSM- 5 have been added for comparison reasons[26].

Catalyst	Temperature (ºC)	k_1 ($L \cdot h^{-1} \cdot mol^{-1}$)	k_2 ($L \cdot h^{-1} \cdot mol^{-1}$)	k_{D_LA} ($L^{1.5} \cdot h^{-1} \cdot mol^{-1.5}$)	k_{D_FFL} (h^{-1})	k_{D_β} (h^{-1})	k_{D_δ} (h^{-1})	r^2
Amb IR-120	**125°C**	0.041	–	0.416	0.020	–	–	
Amb-36	**125°C**	0.045	–	0.213	0.034	–	–	
ZSM-5 (23)								
	125°C	0.076	0.003	0.038	0.026	–	–	0.992
	150°C	0.198	0.026	0.056	0.043	–	–	0.985
	175°C	0.725	0.224	0.273	0.271	0.054	0.003	0.958
	Ea ($kJ \cdot mol^{-1}$)	72.1	128	–	–	–	–	–
	A (s^{-1})	$1 \cdot 10^4$	$3 \cdot 10^{10}$					
	r^2	0.992	0.999					
MCM								
	125°C	0.090	0.014	–	–	–	–	0.986
	150°C	0.256	0.104	0.106	0.051	–	–	0.996
	175°C	1.225	0.327	0.312	0.222	0.082	–	0.973
	Ea ($kJ \cdot mol^{-1}$)	77.1	93.4					
	A (s^{-1})	$3 \cdot 10^5$	$8 \cdot 10^6$					
	r^2	0.978	0.986					
Al_2O_3								
	125°C	0.142	0.017	–	0.021	–	–	0.999
	150°C	0.518	0.098	–	0.077	0.032	–	0.994
	175°C	1.625	0.474	–	0.388	0.080	–	0.991
	Ea ($kJ \cdot mol^{-1}$)	72.4	98.7					
	A (s^{-1})	$2 \cdot 10^4$	$1 \cdot 10^7$					
	r^2	0.999	0.999					

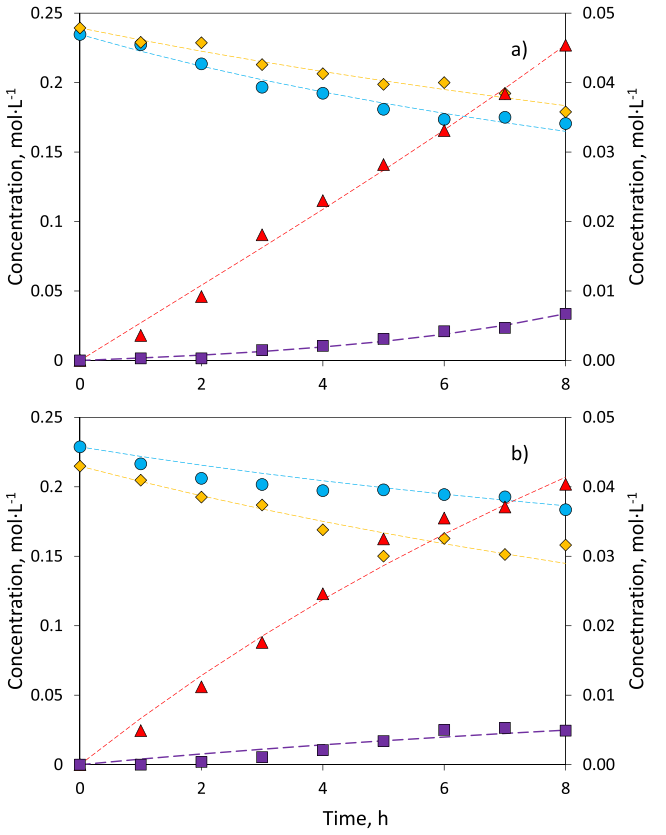

Fig. 4. Temporal evolution of FFL (♦), NaLe (●); β-C10 (▲), and δ-C10 (■) during the FFL-NaLe (1:1) aldol condensation at 125 °C catalyzed by 7.2 g/L of (a) MCM, and (b) Al_2O_3. *Reactants must be read in the left axis, products in the right one. Symbols correspond to experimental points, whereas broken lines indicate the concentrations predicted by the kinetic model.*

can be reached with a variety of temperatures and times, including also points that correspond to good carbon balances (95.7 %). These values correspond to 7–8 h of reaction at 150 °C, conditions defined as the optimum ones with this material. As to MCM, the maximum of C10 is slightly lower (43.2 %), and it is reached at CSF values high enough to produce a significant decrease in the carbon balance (values close to 70 %). According to this analysis, Al_2O_3 is defined as the optimum material, as well as 150ºC the optimum temperature to maximize the C10 production without being affected by side reactions.

3.3. Kinetic study

The temporal evolution of the compounds involved in these reactions was fitted to the kinetic model proposed in our previous work (Cueto et al., 2020), illustrated in Scheme 1. To sum up, two parallel reactions are considered, as a function of the site of proton abstraction: either on the tertiary carbon, producing the branched compound (β-C10) or on the terminal one, obtaining the less stable linear adduct (δ-C10). In both cases, global second order is considered. The adsorption of both reactants, as well as the oligomerization of both products (obtaining precipitates, not detected by the analytical method), is considered as four lateral reactions, with first order dependence in all the cases, except for the NaLe one, in good agreement with the oligomerization trend previously indicated. This model is summarized in the following differential equations:

$$\frac{d(LA)}{dt} = -k_1 \cdot C_{LA} \cdot C_{FFL} - k_2 \cdot C_{LA} \cdot C_{FFL} - k_{D_{LA}} \cdot C_{LA}^{2.5} \quad (5)$$

$$\frac{d(FFL)}{dt} = -k_1 \cdot C_{LA} \cdot C_{FFL_{1:1}} - \quad k_2 \cdot C_{LA} \cdot C_{FFL} - k_{D_{FFL}} \cdot C_{FFL} \quad (6)$$

$$\frac{d(\beta - C10)}{dt} = k_1 \cdot C_{LA} \cdot C_{FFL} - k_{D_\beta} \cdot C_{\beta C10} \quad (7)$$

$$\frac{d(\delta - C10)}{dt} = k_2 \cdot C_{LA} \cdot C_{FFL} - k_{D_\delta} \cdot C_{\delta C10} \quad (8)$$

The kinetic rates are shown in Table 2 (including those obtained with ZSM-5, for comparison purposes), whereas Fig. 4 shows the good correspondence between experimental and fitted values obtained with all the materials at 125 °C.

Kinetic constants obtained support the previous discussions. Thus, resins are discarded for deeper studies since they mainly promote the adsorption of both reactants, obtaining the lowest k_1 values. The two aldol condensation reactions have bigger kinetic constants with mesoporous materials than with the ZMS-5. The k_1/k_2 ratios are in good agreement with the β/δ ratios, suggesting that the β/δ ratio is due to a prevalence of the first mechanism over the second one, discarding possible adsorptions or lateral reactions involving any of these compounds.

Fig. 5 illustrates the good correspondence between experimental and fitted values at 150 and 175 °C. As expected, both parallel reactions follow the Arrhenius model, obtaining activation energies in the typical range of catalytic processes. With both materials, the activation energy of the linear adduct (from 93.4 to 128 kJ·mol^{-1}) is higher than the branched one (from 72 to 77 kJ·mol^{-1}), fact due to the lower stability of the enol obtained when the proton abstraction occurs on the terminal carbon. In terms of activation energy, the substitution of a microporous zeolite with mesoporous materials significantly reduces the barrier needed to cross the transition state threshold of the linear adduct, observing a reduction of more than 23 %. The absence of mass transfer limitations in mesoporous materials justifies these decreases since these diffusional effects mainly affect the δ-C10 molecule (the biggest one). On the contrary, an almost negligible effect is observed for the β-C10 formation rate (k_1), with differences lower than 7 %.

The best results obtained with MCM and, mainly, Al_2O_3 are then a combination of a significant reduction in lateral reactions (mainly at low temperatures) and, for the β-C10, the increase in the pre-exponential value, the empirical factor of the Arrhenius model related to the entropy contribution, that in the context of heterogeneous catalysis is related to the reactants' approach to the active site, i.e., the accessibility of these sites (Slot et al., 2020).

The lack of correspondence between kinetic rates and total acidity supports the previous hypothesis about the negative effect of Brønsted acidity. The lack of correspondence is also observed when considering weak, medium-strength, or strong sites, discarding the strength of the active sites as a relevant parameter. On the contrary, there is a clear correspondence between the concentration of Lewis sites and the k_1 values, despite the temperature analyzed, see Fig. 6. There is no decisive conclusion related to the k_2 rate (δ-C10), which can be due to the low accuracy of the kinetic model fitting such low concentrations.

3.4. Stability study

TPO analyses of the spent catalysts were done to characterize the nature of the possible organic deposits that explain the depletion in the carbon balance closure. Fig. 7 shows the profiles of the CO_2 signals with the temperature. The corresponding analysis with the resins is not possible because of the thermal instability of these materials. The highest CO_2 release is obtained with ZSM-5, the total amount being three times higher than the corresponding ones obtained with Al_2O_3 and MCM, respectively.

These differences are not only relevant in quantitative terms but also to the stability of these organic deposits, a parameter that is directly

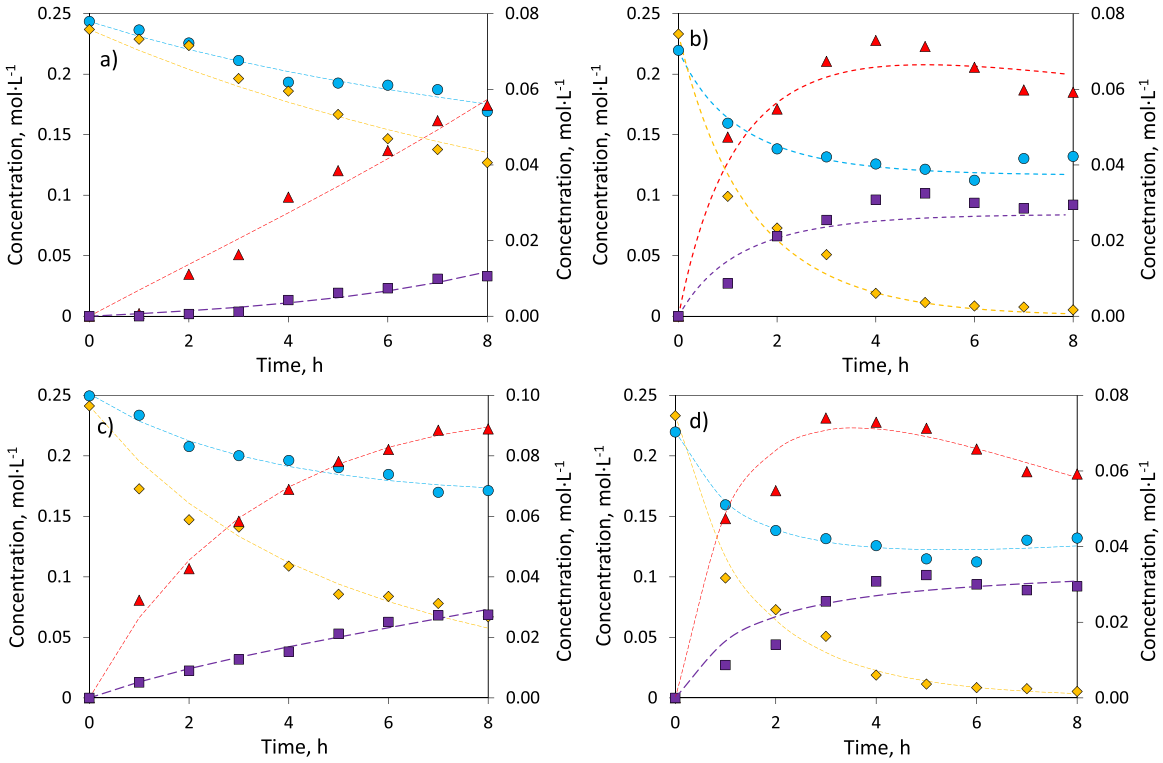

Fig. 5. Temporal evolution of FFL (♦), NaLe (●); β-C10 (▲), and δ-C10 (■) during the FFL-NaLe (1:1) aldol condensation as a function of the temperature and catalyst used. (a) MCM, 150 °C; (b) MCM, 175 °C; (c) Al_2O_3, 150 °C; and (d) Al_2O_3, 175 °C. *Reactants must be read in the left axis, products in the right one. Symbols correspond to experimental points, whereas broken lines indicate the concentrations predicted by the kinetic model.*

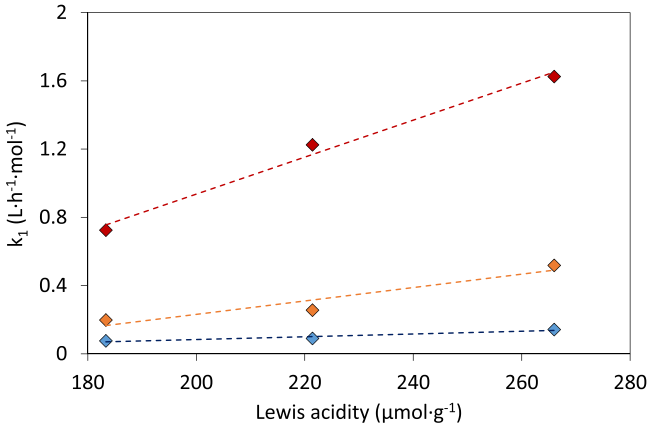

Fig. 6. Kinetic rate constant of the β-C10 formation as a function of the Lewis acidity of the different catalysts. Data correspond to results at 125 °C (blue), 150 °C (orange), and 175 °C (red).

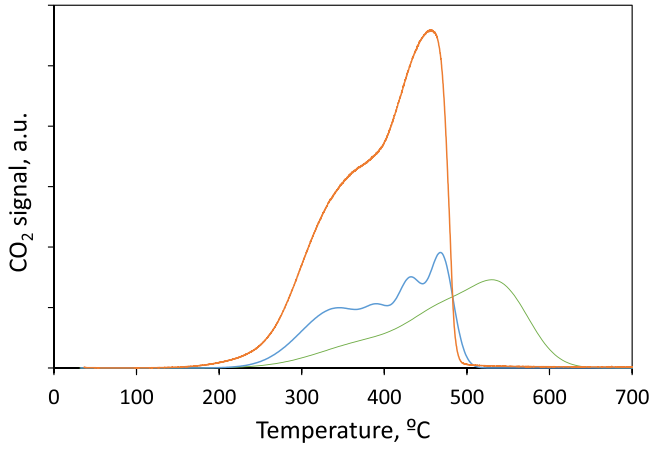

Fig. 7. TPO analyses of the spent catalyst recovered after 8 h of reaction at 150 °C: ZSM-5 (orange), MCM (blue), and Al_2O_3 (green). *Results normalized by mass of catalyst.*

related to the strength of the interactions between the compound adsorbed and the material. TPO analyses of these materials after saturating their surface with NaLe and FFL discard relevant differences due to the interactions with the supports, discarding a relevant effect of mass transfer limitation with ZSM-5. Thus, the TPO of materials saturated in FFL produces a CO_2 signal in the range 250–380 °C whereas the TPO of the materials after the impregnation with NaLe demonstrates stronger adsorption, the decomposition temperatures increasing to 350–490 °C.

According to these analyses, and in good agreement with the kinetic model proposed, the decrease in the carbon balance is mainly due to the adsorption of the reactants in the cases of ZSM-5 and MCM. In this last case, the presence of different peaks at similar temperatures could suggest the adsorption of other compounds, the products being the main candidates. The lack of commercial samples of these compounds makes impossible the corresponding adsorption analyses. The CO_2 signal obtained with Al_2O_3 at these temperatures is significantly lower, but the relevant peak at 540 °C suggests the presence of organic compounds strongly adsorbed. The flat evolution of the main product (β-C10) suggests that this peak could correspond to the oxidation of this compound. In any case, the decomposition temperature is lower than the activation one, the thermal and chemical stability of the catalyst being guaranteed, suggesting that the reusability is possible if the material is regenerated at 550 °C after each reaction cycle.

Considering these results, the stability analysis of the most promising material (Al_2O_3) was done at 150 °C, limiting the reaction time to 6 h.

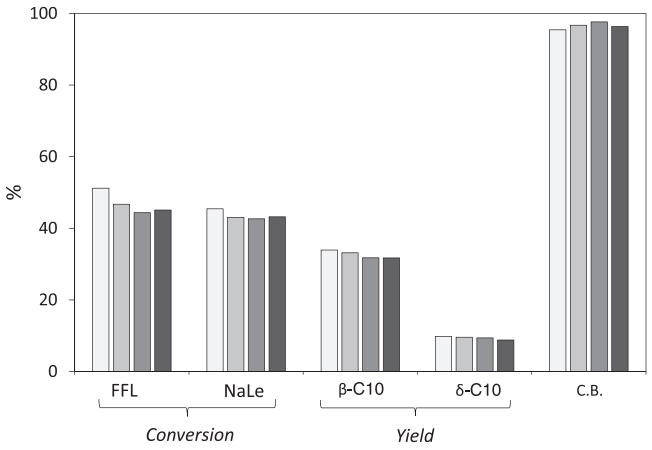

Fig. 8. Reusability analysis of Al_2O_3 for the NaLe:FFL aldol condensation. Results after 6 h at 150 °C.

Longer times were discarded since the C10 production is almost stable since the first 5 h, suggesting that after this time, the most effective acid sites for the aldolization are significantly blocked. Fig. 8 summarizes the main results obtained.

Experimental results demonstrate that Al_2O_3 can be reused for at least four cycles without suffering deactivation (with regeneration between cycles), with a decrease in the total C10 production lower than 6.5 % after these four cycles. The good carbon balance closures obtained corroborate the efficiency of the regeneration process oxidizing the possible organic solids and reactivating the active sites. Thus, according to activity and stability tests, Al_2O_3 is proposed as a promising catalyst for the furfural and levulinic acid cross condensations (levulinic acid being previously esterified with Na_2CO_3) at 150 °C, being an available and cheap material that can ensure the economic feasibility of this approach to obtain liquid-fuel precursors.

4. Conclusion

We have demonstrated that γ-Al_2O_3 (a cheap and commercially available catalyst) has a great activity as an acid catalyst for the aldol condensation of furfural and levulinic acid, two of the top ten biomass-derived compounds. Levulinic acid must be esterified before the reaction to passivate the activity of the carboxylic functional group, the aldol condensation being carried out with sodium levulinate (NaLe). After 6 h at 150ºC, Al_2O_3 allows the selective production of β- and δ-C10 adducts (liquid fuel precursors), with high activity (>40 % of NaLe conversion). The good carbon balance (>95 %) discards a high relevance of adsorption processes, with the corresponding high stability observed in the reusability tests (four tests with a constant 44 % of C10).

The mesoporous aluminosilicate MCM-41 also shows a good activity, but more severe conditions are required to obtain similar results (C10 total yield of 39 % after 24 h at 175 °C), and the NaLe adsorption is significantly more relevant than with the Al_2O_3. The activity of ion-exchange resins is discarded since the strong adsorption obtained prevents the production of the desired products and the thermal instability of these materials discards working at higher temperatures to reduce the role of this adsorption.

Experimental results perfectly fit with the reaction kinetic model proposed for microporous materials, suggesting the Lewis weak and medium acidity as the main active sites to promote the condensation.

CRediT authorship contribution statement

Jennifer Cueto: Investigation, Methodology, Writing – original draft. **Laura Faba:** Formal analysis, Data curation, Writing – original draft. **Eva Díaz:** Formal Analysis, Data curation. **Salvador Ordóñez:** Conceptualization, Writing – review & editing, Funding acquisition.

Declaration of Competing Interest

The authors declare that they have no known competing financial interests or personal relationships that could have appeared to influence the work reported in this paper.

Data Availability

Data will be made available on request.

Acknowledgements

This work has been funded by the Spanish Ministry of Science and Innovation, Spanish Agency for Research AEI (PID2020-112587RB-I00) and the Regional Government of Asturias (AYUD/2021/50450).

References

Amarasekara, A.S., Singh, T.B., Larkin, E., Hasan, M.A., Fan, H.-J., 2015. NaOH catalyzed condensation reactions between levulinic acid and biomass derived furan-aldehydes in water. Ind. Crop. Prod. 65, 546–549. https://doi.org/10.1016/j.indcrop.2014.10.005.

Amarasekara, A.S., Wiredu, B., Grady, T.L., García Obregón, R., Margetic, D., 2019. Solid acid catalyzed aldol dimerization of levulinic acid for the preparation of C10 renewable fuel and chemical feedstock. Catal. Commun. 124, 6–11. https://doi.org/10.1016/j.catcom.2019.02.022.

Cai, C.M., Zhang, T.Y., Kumar, R., Wyman, C.E., 2014. Integrated furfural production as a renewable fuel and chemical platform from lignocellulosic biomass. J. Chem. Technol. Biotechnol. 89, 2–10. https://doi.org/10.1002/jctb.4168.

Chheda, J.N., Huber, G.W., Dumesic, J.A., 2007. Liquid-phase catalytic processing of biomass-derived oxygenated hydrocarbons to fuels and chemicals. Angew. Chem. Int. Ed. 46, 7164–7183. https://doi.org/10.1002/anie.200604274.

Choudhury, A.R., Mukherjee, S., 2020. Deconjugated butenolide: a versatile building block for asymmetric catalysis. Chem. Soc. Rev. 49, 6755–6788. https://doi.org/10.1039/c9cs00346k.

Cueto, J., Faba, L., Díaz, E., Ordóñez, S., 2017. Performance of basic mixed oxides for aqueous-phase 5-hydroxymethylfurfural-acetone aldol condensation. Appl. Catal. B 201, 221–231. https://doi.org/10.1016/j.apcatb.2016.08.13.

Cueto, L., Korobka, V., Faba, L., Díaz, E., Ordóñez, S., 2020. Aldol condensation of biomass-derived levulinic acid and furfural over acid zeolites. ACS Sust. Chem. Eng. 8, 4371–4383. https://doi.org/10.1021/acssuschemeng.9b06636.

Deng, F., Amarasekara, A.S., 2021. Catalytic upgrading of biomass derived furans. Ind. Crop. Prod. 159, 113055 https://doi.org/10.1016/j.indcrop.2020.113055.

Di Bucchianico, D.D., Wang, Y.J., Buvat, J.C., Pan, Y., Moreno, V.C., Leveneur, S., 2022. Production of levulinic acid and alkyl levulinates: a process insight. Green Chem. 24, 614–646. https://doi.org/10.1039/D1GC02457D.

Estevez, R., López-Pedrajas, S., Blanco-Bonilla, F., Luna, D., Bautista, F.M.M., 2015. Production of acrolein from glycerol in liquid phase on heterogeneous catalysts. Chem. Eng. J. 282, 179–186. https://doi.org/10.1016/j.cej.2015.03.018.

Faba, L., Díaz, E., Ordóñez, S., 2012. Aqueous-phase furfural-acetone aldol condensation over basic mixed oxides. Appl. Catal. B 113, 201–211. https://doi.org/10.1016/j.apcatb.2011.11.039.

Faba, L., Díaz, E., Ordóñez, S., 2016. Base-catalyzed condensation of levulinic acid: a new biorefinery upgrading approach. ChemCatChem 8, 1490–1494. https://doi.org/10.1002/cctc.201600064.

Garcés, D., Faba, L., Díaz, E., Ordóñez, S., 2019. Aqueous-phase transformation of glucose into hydroxymethylfurfural and levulinic acid by combining homogeneous and heterogeneous catalysis. ChemSusChem 12, 924–934. https://doi.org/10.1002/cssc.201802315.

Gelbard, G., 2005. Organic synthesis by catalysis with ion-exchange resins. Ind. Eng. Chem. Res. 44, 8468–8498. https://doi.org/10.1021/ie0580405.

He, J., Qiang, Q., Liu, S., Song, K., Zhou, X., Guo, J., Zhang, B., Li, C., 2021. Upgrading of biomass-derived furanic compounds into high-quality fuels involving aldol condensation strategy. Fuel 306, 121765. https://doi.org/10.1016/j.fuel.2021.121765.

Kikhtyanin, O., Chlubná, P., Jindrová, T., Kubicka, D., 2014. Peculiar behaviour of MWW materials in aldol condensation of furfural and acetone. Dalton Trans. 43, 10628–10641. https://doi.org/10.1039/C4DT00184B.

Li, C., Ding, D., Xia, Q., Liu, X., Wang, Y., 2016. Conversion of raw lignocellulosic biomass into branched long-chain alkanes through three tandem steps. ChemSusChem 9, 1712–1718. https://doi.org/10.1002/cssc.201600386.

Li, H., Riisager, A., Saravanamurugan, S., Pandey, A., Sangwan, R.S., Yang, S., Luque, R., 2018. Carbon-increasing catalytic strategies for upgrading biomass into energy-intensive fuels and chemicals. ACS Catal. 8, 148–187. https://doi.org/10.1021/acscatal.7b02577.

Li, X.Y., Xu, R., Liu, Q.L., Liang, M., Yang, J.X., Lu, S.C., Li, G.B., Lu, L.F., Si, C.L., 2019. Valorization of corn stover into furfural and levulinic acid over SAPO-18 zeolites:

effect of Bronsted to Lewis acid sites ratios. Ind. Crop. Prod 141, 11759. https://doi.org/10.1016/j.indcrop.2019.11759.
Liang, G., Wang, A., Zhao, X., Lei, N., Zhang, 2016. Selective aldol condensation of biomass-derived levulinic acid and furfural in aqueous-phase over MgO and ZnO. Green Chem. 18, 3430–3438. https://doi.org/10.1039/C6BC00118A.
Malkar, R.S., Daly, H., Hardacre, C., Yadav, G.D., 2019. Aldol condensation of 5-hydroxymethylfurfural to fuel precursors over novel aluminium exchanged-DTP@ZIF-8. ACS SUS. Chem. Eng. 7, 16215–16224. https://doi.org/10.1021/acssuschemeng.9b02939.
Mascal, M., Dutta, S., Gandarias, I., 2014. Hydrodeoxygenation of the angelica lactone dimer, a cellulose-based feedstock: simple, high-yield synthesis of branched C7-C10 gasoline-like hydrocarbons. Angew. Chem. Int. Ed. 53, 1854–1857. https://doi.org/10.1002/anie.201308143.
Nieminen, V., Karhu, H., Kumar, N., Heinmaa, I., Ek, P., Samoson, A., Salmi, T., Murzin, D.Yu, 2004. Physico-chemical and catalytic properties of Zr- and Cu-Zr ion-exchanged H-MCM-41. Phys. Chem. Chem. Phys. 6, 4062–4069. https://doi.org/10.1039/B404176C.
Pasricha, S., Gahlot, P., Mittal, K., Rai, D., Avasthi, N., Kaur, H., Rai, S., 2022. Functionalized MCM-41: versatile catalysts for organic transformations. Chemistryselect 7, e202103674. https://doi.org/10.1002/slct.202103674.
Perego, C., Millini, R., 2013. Porous materials in catalysis: challenges for mesoporous materials. Chem. Soc. Rev. 42, 3956–3976. https://doi.org/10.1039/C2CS35244C.
Ramírez, E., Bringué, R., Fité, C., Iborra, M., Tejero, J., Cunill, F., 2017. Role of ion-exchange resins as catalyst in the reaction-network of transformation of biomass into biofuels. J. Chem. Technol. Biotechnol. 92, 2775–2786. https://doi.org/10.1002/jctb.5352.
Rapado, P., Faba, L., Ordóñez, S., 2021. Influence of delignification and reaction conditions in the aqueous phase transformation of lignocellulosic biomass to platform molecules. Bioresour. Technol. 321, 124500 https://doi.org/10.1016/j.biortech.2020.124500.
Russo, V., Rossano, C., Salucci, E., Tesser, R., Salmi, T., Di Serio, M., 2020. Intraparticle diffusion model to determine the intrinsic kinetics of ethyl levulinate synthesis promoted by Amberlyst-15. Chem. Energy Sci. 228, 115974 https://doi.org/10.1016/j.ces.2020.115974.
Schekler-Nahama, Clause, O., Commereuc, D., Saussey, J., 1998. Influence of Lewis acidity of rhenium heptoxide supported on alumina catalyst on the catalytic performances in olefin metathesis. Appl. Catal. A 167, 237–245. https://doi.org/10.1016/S0926-860X(97)00310-4.
Slot, T.K., Riley, N., Shiju, N.R., Medlin, J.W., Rothenberg, 2020. An experimental approach for controlling confinement effects at catalyst interfaces. Chem. Sci. 11, 11024–11029. https://doi.org/10.1039/d0sc04118a.
Su, M., Li, W., Ma, Q., Li, S., Yang, T., Duo, X., 2019. Efficient synthesis of liquid fuel intermediates from furfural and levulinic acid via aldol condensation over hierarchical MFI zeolite catalyst. Energy Fuels 33, 12518–12526. https://doi.org/10.1021/acs.energyfuels.9b03307.
Tan, J., Wang, C., Zhang, Q., Ma, L., He, M., 2018. One-pot condensation of furfural and levulinate: a novel methos for cassava use in synthesis of biofuel precursors. . Energy Fuels 32, 6807–6812. https://doi.org/10.1021/acs.enegyfuels.8b0396.
Wang, D., Hakim, S.H., Alonso, D.M., Dumesic, J.A., 2013. A highly selective route to linear alpha olefins from biomass-derived lactones and unsaturated acids. Chem. Commun. 49, 7040–7042. https://doi.org/10.1039/C3CC43587C.
Wang, Z.X., Bhattacharyya, S., Vlachos, D.G., 2021. Extraction of furfural and furfural/5-hydroxymethylfurfural from mixed lignocellulosic biomass-derived feedstocks. ACS Sust. Chem. Eng. 9, 7489–7498. https://doi.org/10.1021/acssuschemeng.1c00982.
Wen, W.C., Eady, S.C., Thompson, L.T., 2020. Oxide supported metal catalysts for the aldehyde water shift reaction: elucidating roles of the admetal, support, and synergies. Catal. Today 355, 199–204. https://doi.org/10.1016/j.cattod.2019.03.064.
Werpy, T., Peterson, G., 2004. Top value-added chemicals from biomass. Volume I – Results of screening for potential candidates from sugars and synthesis gas. Natl. Renew. Energy Lab. (NREL).
Xu, J., Yang, X., Li, G., Wang, A., Cong, Y., Wang, X., Zhang, T., 2017. Synthesis of diesel and jet fuel range alkanes with furfural and angelica lactone. ACS Catal. 7, 5880–5886. https://doi.org/10.1021/acscatal.7b01992.
Xue, Z.M., Liu, Q.L., Wang, J.F., 2018. Valorization of levulinic acid over non-noble metal catalysts: challenges and opportunities. Green Chem. 20, 4391–4408. https://doi.org/10.1039/c8gc02001a.
Zhang, L., Xi, G., Yu, K., Yu, H., Wang, X., 2017. Furfural production form biomass-derived carbohydrates and lignocellulosic residues via heterogeneous acid catalysts. Ind. Crop Prod. 98, 68–75. https://doi.org/10.1016/j.indcrop.2017.01.014.
Zhao, X.L., Li, S., Hu, Y.Z., Zhang, X.H., Chen, L.G., Wang, C.G., Ma, L.L., 2021. Synthesis of long chain alkanes via aldol condensation over modified chitosan catalyst and subsequent hydrodeoxygenation. Chem. Eng. J. 428, 131368 https://doi.org/10.1016/j.cej.2021.131368.
Zhi, Z.H., Li, N., Qiao, Y.N., Zheng, X.J., Wang, H.T., Lu, X.B., 2015. Kinetic study of levulinic acid production from corn stalk at relatively high temperature using FeCl3 as catalyst: a simplified model evaluated. Ind. Crop. Prod. 76, 672–680. https://doi.org/10.1016/j.indcrop.2015.07.058.